Atomization and Sprays, 22 (7): 581–601 (2012)

VACUUM-ASSISTED GAS ATOMIZATION OF LIQUID METAL

S. P. Mates,[1,*] S. D. Ridder,[1] F. S. Biancaniello,[1] & T. Zahrah[2]

[1]*National Institute of Standards and Technology, Gaithersburg, MD, 20899, USA*

[2]*MATSYS, Inc., Sterling, VA, 20166, USA*

[*]Address all correspondence to S. P. Mates E-mail: smates@nist.gov

Original Manuscript Submitted: 6/30/2012; Final Draft Received: 10/18/2012

Vacuum-assisted gas atomization of liquid metal is explored. The investigation is motivated by observations of liquid metal atomization that indicate that secondary atomization is sustained over an extended distance from the nozzle tip. Increasing the velocity of the gas flow downstream of the nozzle exit by lowering the nozzle back pressure below ambient may therefore improve atomization efficiency. Supersonic jets grow in length when the nozzle back pressure is lowered due to an increase in the nozzle pressure ratio. However, since the nozzle mass flux remains fixed, any improvements in vacuum-assisted atomization efficiency will be realized without any increase to the gas-to-metal mass flow ratio, which is of interest both academically and practically as gas consumption can be costly. Small (25-kg batch) atomization runs were performed using an Al-Cu-Ni glass-forming alloy in which a high-mass-flow vacuum system was employed to maintain a sub-ambient chamber pressure over the course of an entire run. The powder produced in this manner was then compared to the conventional method without the vacuum system operating. Results demonstrate that atomizing into a partial vacuum decreases the frequency of the coarsest particles in the powder size distributions, leading to a narrower particle size distribution. Further, they underscore the importance of the axial length scale affecting secondary atomization that is related to, but not fully described by, the gas-to-liquid mass flux ratio. The present experiments point out a significant and unexplored parameter space that may be exploited to increase control over particle size distributions.

KEY WORDS: *gas atomization, metal powder, particle size control*

1. INTRODUCTION

Gas atomization of molten metal is a preferred method for producing high-quality spherical metal powders with low oxygen content for use in advanced manufactured parts using powder metallurgy processing techniques (German, 2005). Other applications of note for these powders include electronic solder paste, paints and pigments, rocket propellants, and raw material for additive manufacturing. The premium often placed on very fine (<50 μm) powders has long motivated efforts to improve the fine particle yields through

 © 2012 by Begell House, Inc.

understanding and enhancing aerodynamic breakup (Ayers and Anderson, 1986; Klar and Fesko, 1984; Ridder and Biancaniello, 1988; Thompson, 1948; Ünal and Robertson, 1986). Through the efforts of these and other researchers, much has been learned about the physics of this rather unique application within the larger arena of twin-fluid atomization with applications such as combustion (Lefebvre, 1989). Much past effort to reduce or influence particle size (increase atomization "efficiency") has been dominated by efforts to enhance primary breakup at or very near the nozzle tip, motivated largely by early fluid dynamic studies of atomization of viscous non-metallic liquids (Dombrowski and Johns, 1963). Efforts to enhance breakup conditions here have focused on nozzle tip shape (Klar and Fesko, 1984; Miller et al., 1997; Mullis et al., 2011; Ünal, 1988), using trumpet-shaped nozzles (Anderson et al., 2010) or linear arrangements (Walz, 1984) to thin the liquid stream as much as possible prior to its interaction with the atomizing gas at the nozzle exit. Such efforts parallel those in fuel injector design, within the considerable additional restrictions of having to deal with molten liquids with a propensity to freeze solid and block the nozzle, which severely limits the scope of viable atomizer geometries. Powerful computational analysis methods are ever more frequently applied to better understand atomization mechanisms and design improved nozzles (Markus and Fritsching, 2006; Tong and Browne, 2009; Zeoli et al., 2012; Zhao et al., 1012).

Secondary atomization, by contrast, although generally considered important to this process, has received less focus for its potential role in refining particle size and controlling droplet size distributions. The importance of secondary breakup has been revealed by high-speed photography of atomization plumes and been analyzed in detail (Mates and Settles, 2005a; Ünal, 1989; Yule and Dunkley, 1994). Droplets that are atomized well beyond the nozzle tip region will generally experience less aggressive aerodynamic conditions due to gas velocity decay, leading to coarser particles and wider particle size distributions. The mechanisms of turbulent mixing and droplet drag that cause gas velocity decay give rise to the conceptual model of liquid metal atomization shown in Fig. 1, which is based on spray plume observations and emphasizes an extended secondary breakup zone. Figure 1 shows Schlieren images (Settles, 2001) that indicate the extent of the supersonic gas flow region with and without liquid present, the latter using stop-motion microsecond-duration lighting (Mates and Settles, 2005a). Primary atomization of the liquid core appears to be complete within about one nozzle diameter. Secondary atomization apparently continues over an extended distance, as indicated by the appearance of large, incompletely atomized droplets well beyond the primary atomization zone. The Schlieren technique reveals qualitatively how the gas velocity decays significantly over this distance: as the gas density approaches that of the surroundings as it decelerates from supersonic speeds, the initially bright gas plume gradually blends into the background. Thus the large droplets that escape primary atomization intact eventually break down under much reduced aerodynamic driving forces due to the decaying gas velocity, which occurs by turbulent mixing with the surrounding gas and by drag exerted by the liquid.

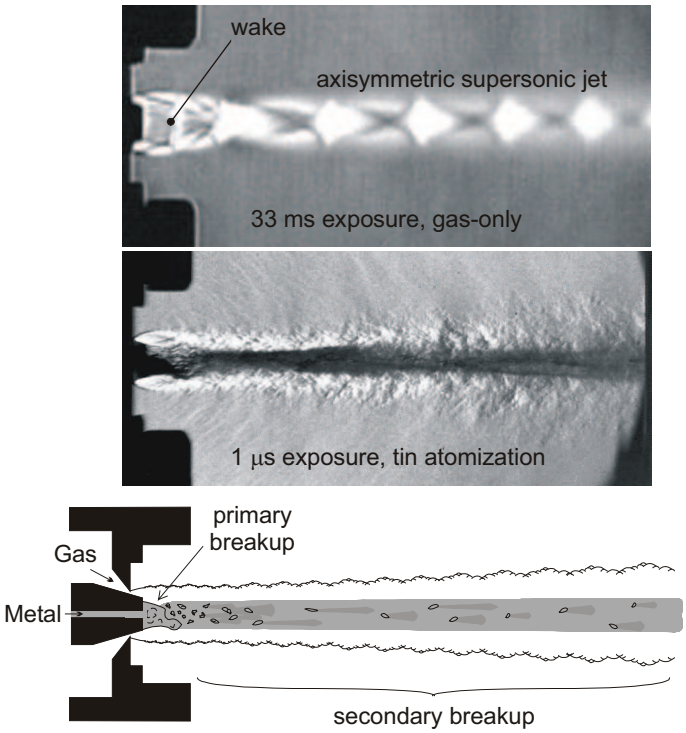

FIG. 1: Top: long-exposure Schlieren image of gas-only operation using a convergent nozzle. Middle: microsecond-exposure Schlieren image of metal atomization showing large un-atomized liquid ligaments (dark spots in center of jet) existing well downstream of the nozzle tip. Bottom: conceptual sketch of atomization process showing a short primary breakup region and an extended secondary breakup zone.

Overall, the conceptual model of liquid metal atomization in Fig. 1 compares very well with what has been observed in subsonic co-flowing atomizers when the gas momentum flux is two orders of magnitude larger than the liquid momentum flux and the liquid Reynolds number is low. It has been called the "recirculating gas cavity" breakup regime in a comprehensive review of twin-fluid atomization (Lasheras and Hopfinger, 2000), including an extended region of secondary breakup. Further, the importance of secondary atomization in determining the median droplet size is evident in the form of the empirical models developed to describe the behavior of these atomizers. Many highly cited models involve terms proportional to the gas-to-liquid flow ratio, either mass-based (Kim and Marshall, 1971; Lefebvre, 1991; Lubanska, 1970) or volume-based (Dunkley, 2001; Nukiyama and Tanasawa, 1938–40). However, the literature also suggests that such ratios have no fundamental role in promoting liquid instability. Many experimental studies demonstrate that the outcome of atomization can be fully described by intensive properties of the gas and liquid alone (Adelberg, 1968; Hsiang and Faeth, 1993; Wigg,

1964), including velocity, density, viscosity, surface tension, although a characteristic length scale, such as droplet diameter, is needed as well. Such experiments invariably involve the breakup of liquid droplets or streams injected into wind tunnels, where the gas flux dwarfs that of the liquid. Despite the fact that the local gas flow around a disintegrating liquid droplet is very complex, the drop size distributions have nevertheless been successfully predicted from "freestream" aerodynamic conditions in these cases. Thus, in this case the amount of gas or liquid plays no role, proving that gas-to-liquid ratio has no intrinsic influence on liquid instability.

The situation is dramatically different, however, for twin-fluid atomization processes, like the present one, where the gas and liquid flow rates are of the same order of magnitude. A range of sensitivity of droplet size to gas-to-liquid ratio of between 0.1 and 10 was suggested in Kim and Marshall (1971). For metal powder production, the gas-to-metal ratios (GMRs) are typically of order 1 (Lawley, 1992; Yule and Dunkley, 1994) due to economics, which favors high production rates (metal flow rates) and thus low GMRs. An added bonus is that large metal flow rates prevent freeze-offs. As shown earlier, in this range of limited GMR, the freestream driving force decays significantly along the length of the plume, due to turbulent mixing and liquid drag. Thus, the use of GMR in these models may have been a way to account for this *axial* length scale effect that influences atomization performance in this regime. To illustrate, considering the gas flow by itself, it is known that, for supersonic atomization nozzles, the supersonic length of the jet is proportional to the gas mass flow rate (Nagamatsu et al., 1996). Second, as demonstrated in subsonic co-flowing atomization of conventional (low freezing temperature) liquids at high gas-to-liquid momentum ratios, the extent of the secondary atomization zone is influenced by the liquid mass flux (Lasheras and Hopfinger, 2000). Thus, within this range, atomization efficiency can be influenced by altering secondary atomization conditions, in ways not suggested by the more usual focus on primary atomization. According to the established empirical models, the most effective way to reduce the mean particle size is to simply increase GMR. Here, however, we attempt to influence this axial length scale independent of GMR, by lowering the pressure of the atomization chamber to increase the extent of the supersonic region without any additional gas mass flow, in what we call vacuum-assist.

By virtue of the large nozzle stagnation pressures (P_0) typically used to atomize liquid metal, the gas flow is substantially supersonic, and extended supersonic jets are typical. This is true regardless of whether the nozzle is of "sonic" (convergent) design or of "supersonic" (convergent–divergent) design. For example, the supersonic jet shown in Fig. 1 is produced by a convergent, "sonic" nozzle. It produces an under-expanded supersonic jet of high Mach number, but with a series of repeating shock cells. Despite this under-expanded condition, this nozzle can produce a supersonic jet of similar length to a convergent–divergent nozzle due its annular, rather than round, gas orifice (Mates and Settles, 2005b). One method to enhance the supersonic jet length is to lower the pressure of the environment into which the nozzle exhausts, called the nozzle "back pressure."

Here this is the pressure in the atomizing chamber, P_{ac}. In many industrial gas atomizers including the one used here, the spray plume is contained in an environmentally controlled chamber to limit oxygen pickup in the metal powder. Typically, the pressure in this chamber is at or slightly above ambient. By lowering P_{ac} to well below this level, the overall pressure ratio across the gas nozzle is increased, leading to greater expansion of the gas and an elongated supersonic jet. For round nozzles, supersonic jet length is related to the pressure ratio P_0/P_{ac} (Nagamatsu et al., 1996):

$$\frac{L_{\text{sonic}}}{D} = \frac{10}{\gamma - 1}\left[\left(\frac{P_0}{P_{\text{ac}}}\right)^{\frac{\gamma-1}{\gamma}} - 1\right] + 0.8 \tag{1}$$

Once the nozzle throat becomes sonic, its mass flow becomes restricted (choked). Lowering the back pressure therefore increases the length of the supersonic jet without increasing the gas mass flow rate. Any benefits to efficiency that are achieved in this way would cost nothing in terms of added gas flow, and would not necessarily change the gas-to-metal mass flow ratio, although the liquid flow can be influenced by changes to the local aerodynamic conditions at the nozzle tip. It is interesting to note that current empirical models based on GMR would fail to predict a reduction in particle size reduction in this case. In fact, these models would predict a coarsening of particle (or droplet) size, as will be discussed later. As such, a positive demonstration of the vacuum-assist effect will, in addition to the practical benefits of achieving increased process efficiency, provide additional insight into the fundamental nature of this liquid metal atomization process, as well as other twin-fluid atomization processes where the gas-to-liquid momentum flux ratio is large.

To investigate the effect of vacuum-assisted atomization, experiments were conducted using the NIST SiGMA (Supersonic inert Gas Metal Atomizer). This facility is capable of operating with controlled and sustained sub-ambient pressures in the atomizing chamber. Four 25 kg batches of an Al-Cu-Ni alloy were atomized, two with near-ambient pressure maintained in the collection chamber and two having sub-ambient chamber pressure. This particular glass-forming alloy is being investigated for an application relating to ballistic penetrators using powder metallurgy consolidation techniques. Particle size analysis was conducted to determine the effect of the sub-ambient chamber pressure on the atomization efficiency.

2. EXPERIMENTAL

The NIST SiGMA atomizer, described in detail elsewhere (Ridder et al., 1992), is an induction-melt, bottom-pour arrangement with melting and atomization performed under controlled atmosphere. A schematic of the facility is shown in Fig. 2. SiGMA is capable of atomizing 25 kg heats of alloys of up to 2000 K melting temperature at a typical production rate of about 6 kg/min. Special features of the SiGMA atomizer in-

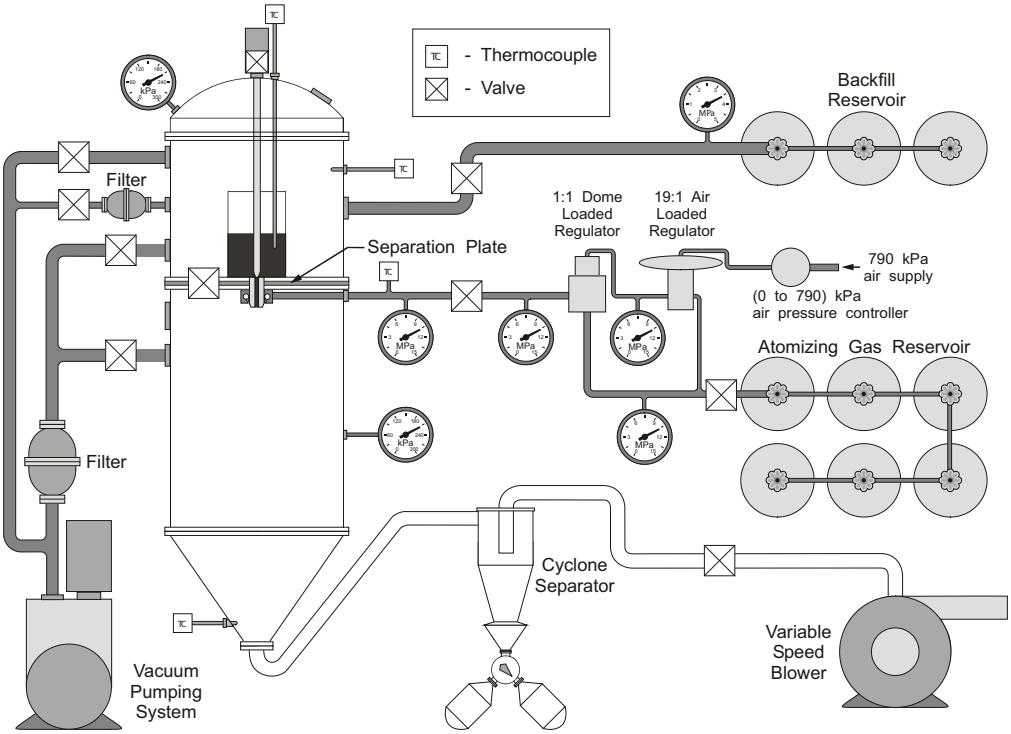

FIG. 2: Schematic of the NIST's SiGMA atomizer facility.

clude feedback control of the gas pressure and the gas-to-metal mass flow ratio. The latter quantity is controlled by monitoring the temperature of the particle-laden exhaust gas stream, which contains the energy of the gas plus molten metal minus losses to the chamber walls (Ridder, 2002). The metal flow rate is adjusted by controlling the pressure in the melt chamber, which can either enhance metal flow or hold it back depending on the chosen liquid pressure differential across the nozzle. Maintaining a constant exhaust gas temperature by continually adjusting the metal flow rate in this manner ensures a constant gas-to-metal ratio during atomization.

Figure 3 shows the multi-jet close-coupled atomization nozzle arrangement used. The liquid metal delivery tube was made from a boron nitride/silicon carbide composite. The gas nozzle consisted of 40 individual precision-drilled holes arranged symmetrically around the delivery tube. The liquid tube, which is fixed to the melt crucible above using ceramic adhesive, is aligned relative to the gas nozzle by adjusting the height of the melt crucible using thin shims.

To achieve a sub-ambient atomization chamber pressure (P_{ac}) during atomization, the chamber is exhausted by an ultra high flow industrial vacuum system with maximum capacity of 0.35 kg/s (657 SCFM) of air, and minimum inlet pressures of 60 kPa (absolute). The vacuum was installed downstream of the cyclone particle separation mod-

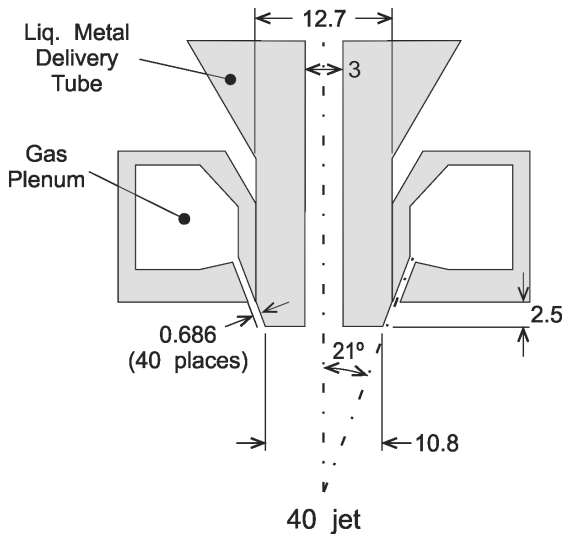

FIG. 3: Gas nozzle assembly. Linear dimensions are in millimeters.

ules, as shown in Fig. 1 (labeled as variable speed blower). With a nominal gas flow of 0.17 kg/s from the nozzle, the amount of gas being injected into the chamber is less than half the throughput capacity of the vacuum system, allowing the chamber pressure to remain at sub-ambient pressures throughout a production run. Figure 4 shows that the atomization chamber can be maintained at about 60% of atmospheric pressure with the vacuum system operating over a wide range of nozzle pressures in the absence of metal flow.

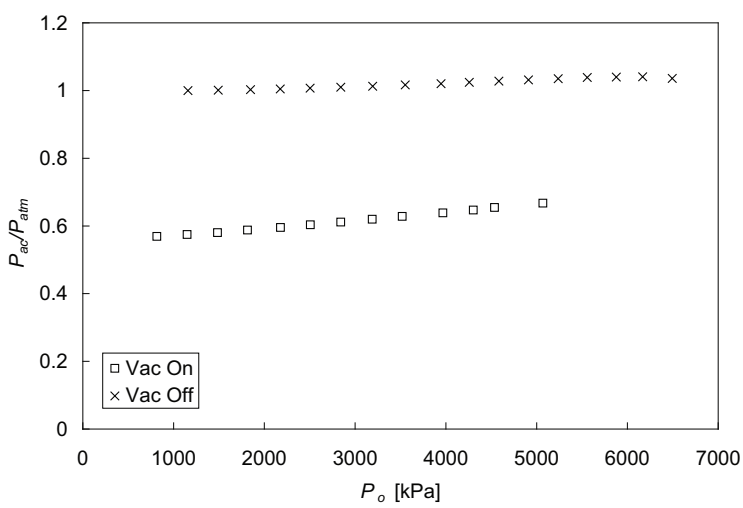

FIG. 4: Atomization chamber pressure ($P_{\rm ac}$) relative to atmospheric pressure ($P_{\rm atm}$) reached with and without the vacuum system activated at various nozzle pressures (P_0).

Particle size analysis was performed using a sonic sieving technique (Biancaniello et al., 1990). The analysis was carried out for particle sizes between 5 μm and 125 μm. Particles larger than 125 μm were removed prior to sieving, while sub–5 μm particles were allowed to pass through the sieve stack. In most cases, only a small amount of material was produced outside the size range analyzed. Because the powder size distributions produced by SiGMA are usually multimodal (Biancaniello et al., 1990), they are not well represented by simple distributions such as the log-normal distribution.

3. RESULTS

Prior to performing atomization experiments at reduced pressures, the nozzle was operated under gas-only conditions with N_2 to identify an operating regime appropriate for atomizing liquid metal. An appropriate regime consists of a range of gas pressures that produce near-ambient to sub-ambient pressures at the tip of the liquid delivery tube. This condition is necessary to allow the liquid metal to flow out of the nozzle, which is often referred to as the aspiration condition, because the nozzle can aspirate metal out of the tundish. Under certain aerodynamic conditions, or if the liquid tube is not properly aligned to the gas nozzle, substantial positive pressures can develop at the nozzle tip, causing the liquid metal flow to arrest and freeze, blocking the tube (a "freeze-off"), or to actively "blow back," two unwanted and possibly dangerous outcomes. Gas-only flow tests were performed into the pressure-controlled atomization chamber with and without the vacuum system in operation to identify an appropriate gas pressure that achieves acceptable aspiration for both normal (ambient) and sub-ambient pressures. The test results are shown in Fig. 5, which plots aspiration pressure, or delivery tube pressure, P_{dt}, against nozzle stagnation pressure, P_0, for two values of P_{ac}: one with the vacuum system operating and one with the vacuum system turned off (normal operation). The two sets of data have similar character, both showing a sudden drop at a particular value of P_0. This phenomenon, known as wake-closure, is associated with a sudden collapse in the subsonic wake zone immediately downstream of the blunt nozzle tip and the formation of a normal shock, or Mach disk, beyond the now-shortened wake zone (Mates and Settles, 2005b). Flow visualization images obtained from a similar annular atomization nozzle are indicated in the figure for illustrative purposes. While seemingly dramatic, this effect usually has little influence on atomization performance because it does not occur when liquid metal is flowing under typical operating conditions because the liquid mass flux raises the pressure in that region substantially. However, it is an important indicator of the range of nozzle pressures where stable metal flow can be achieved, since low nozzle tip pressures act to enhance metal flow and prevent freeze-offs. Based on these aspiration pressure curves, an atomizing pressure of about 6.4 MPa was selected for the experiments. At this value of P_0, the aspiration is well below ambient for both regular and vacuum-assisted operation, indicating good prospects for stable atomization. In Fig. 6, the same aspiration pressure data are plotted against pressure ratio, P_0/P_{ac},

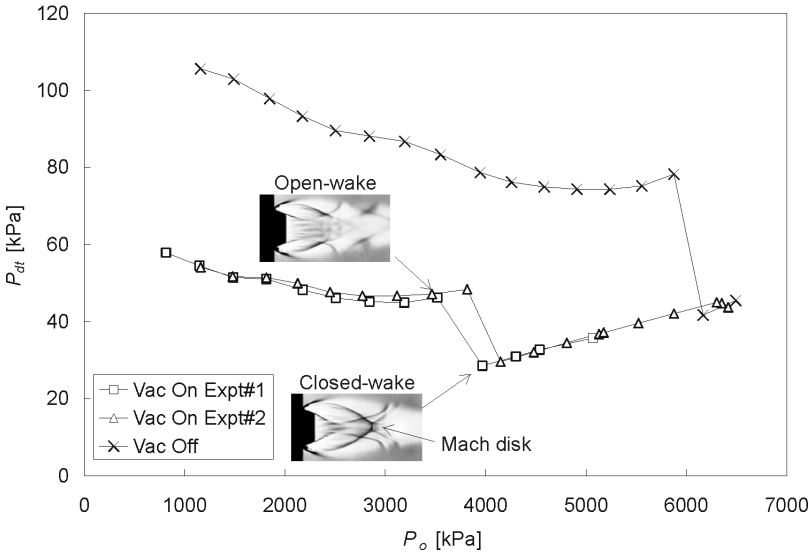

FIG. 5: Effect of atomizer chamber pressure (P_{ac}) on nozzle aspiration behavior (P_{dt}) (Vac On: P_{ac} = 60 $\pm$ 6 kPa; Vac Off: P_{ac} = 101 $\pm$ 3 kPa).

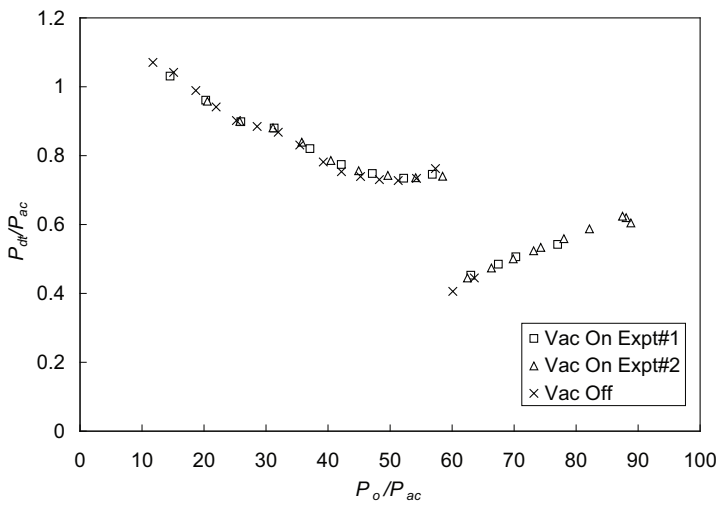

FIG. 6: Aspiration pressure (P_{dt}) plotted against nozzle pressure ratio showing the Mach number dependence of the wake-closure phenomena.

which illustrates that the gas dynamic behavior of the nozzle is fundamentally dependent on the Mach number (M), which is related to pressure ratio through the relation

$$M = \sqrt{\frac{2}{\gamma - 1}\left[\left(\frac{P_0}{P_{\mathrm{ac}}}\right)^{\frac{\gamma-1}{\gamma}} - 1\right]} \tag{2}$$

In the above equation, γ is the specific heat ratio. For nitrogen gas its value is 1.4.

With an acceptable atomizing pressure window identified, four 23-kg batches of CuAlNi were atomized at nozzle stagnation pressures (P_0) between 6.3 MPa and 6.5 MPa and a target GMR of 2.0, representing typical operating conditions for the SiGMA atomizer. Two batches were produced with the vacuum system off, and two with the vacuum system on. Each run took approximately 2.43 minutes to complete. Figure 7 plots the process data obtained for one of the vacuum-assisted atomization runs. As the plot demonstrates, the atomizing parameters are kept nearly constant throughout the run. Only the nozzle stagnation pressure drifts upwards slightly during the run. The vacuum system maintains the chamber at a steady 0.72 atm, slightly higher than the 0.6 atm achieved during gas-only operation. This is thought to be a consequence of the gas temperature increase as heat is extracted from the liquid metal. Also plotted in Fig. 8 is the output from a photosensor pointed at the nozzle tip that is sensitive to the light emission from the molten spray plume. This record indicates the portion of the run where molten metal is flowing.

To roughly quantify the aerodynamic effects of reducing P_{ac}, we compute the properties of equivalent perfectly expanded gas jets at the experimental values of P_0/P_{ac}. Although the actual (imperfectly expanded) jets will differ from these idealized ones, comparing the idealized flow conditions is a good point of reference for anticipating how atomization performance may be affected. The properties of interest include exit velocity, u_{e}, supersonic length, L_{sonic}, gas mass flow rate, m_{gas}, the dynamic pressure, q, and the jet momentum, Q. Values of m_{gas} are obtained from an empirical fit to mass flow versus nozzle pressure data:

$$m_{\mathrm{gas}} = 0.0000266\ P_0 \tag{3}$$

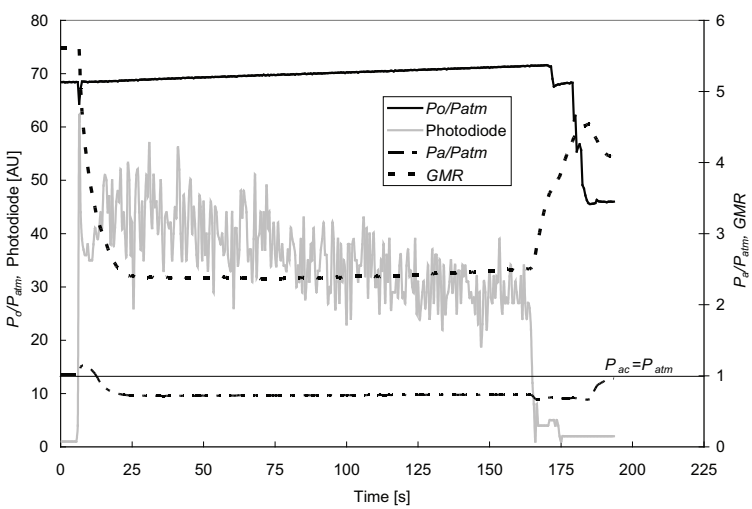

FIG. 7: Process data obtained with vacuum system in operation.

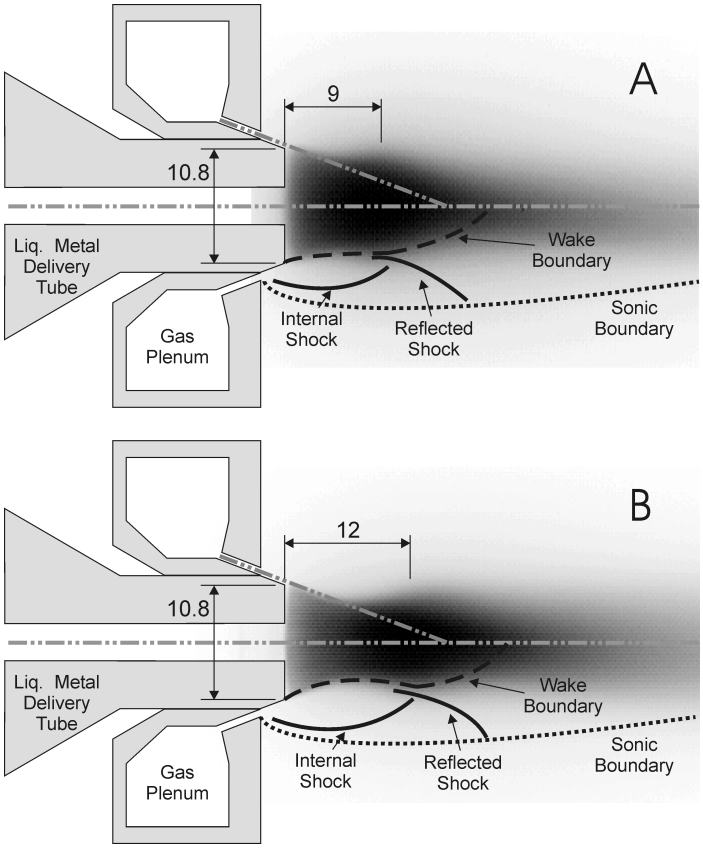

FIG. 8: Time-averaged images of the radiant metal plume (gray levels inverted) at the nozzle tip for normal (A) and vacuum-assisted (B) atomization showing the elongation and narrowing of the plume due to greater gas flow expansion with the reduced chamber pressure. Linear dimensions are in millimeters.

Values of q, u_{e}, and Q are all determined from isentropic relations (White, 1986):

$$q = 0.5\gamma P M^2 \tag{4}$$

$$u_{\mathrm{e}} = M\sqrt{\gamma R T} \tag{5}$$

$$T = \frac{T_0}{1 + \frac{\gamma - 1}{2} M^2} \tag{6}$$

$$Q = m_{\mathrm{gas}} u_{\mathrm{e}}. \tag{7}$$

In Eq. (5), R is the gas constant, which for nitrogen is 297 J/kg·K, and T is the static temperature at the exit condition. T is determined from T_0, the gas stagnation temperature, which is 300 K, using Eq. (6). Ideal aerodynamic conditions corresponding to each

experiment are listed in Table 1. The baseline experiments with no vacuum-assist are labeled B1 and B2, while the vacuum-assisted experiments are labeled VA1 and VA2. Reducing the chamber pressure leads to a 30% increase in L_{sonic}. While the exit velocity and momentum increase slightly, the dynamic pressure drops by 20 %. This is potentially important, since this implies a smaller peak Weber number and thus a larger stable droplet size (Lane, 1951), which works against the goal of achieving more efficient atomization. This will be discussed in more detail below.

In Fig. 8, time-averaged images of the radiant atomization plume show the effect of the reduced chamber pressure on the plume structure. The video data were recorded at 2 frames per second (shutter speed = 1 ms) using a visible light digital video camera. The images are inverted (low gray level indicates high intensity, and vice versa) and contrast enhanced. Beginning at the tip of the liquid delivery tube, the radiant metal plume at first necks down then widens again to an abrupt maximum, after which it gradually narrows again to a point. The metal conforms to this shape due to the aerodynamic forces imposed on it in the nozzle tip region. There exists a region of separated gas flow, sometimes called the wake zone (Mates and Settles, 2005b), which is characterized by low-velocity, swirling motion of the gas. This zone is surrounded by an annular region of high-velocity, supersonic gas flow emanating from the gas orifice ring positioned around the delivery tube. On the border of the wake zone, there can be significant interaction between molten metal and high-speed gas, leading to vigorous atomization. Inside the wake zone, however, very little fine atomization occurs because of the low, swirling gas velocities present. The flow pattern here is also highly disrupted by the presence of large clumps of molten metal. Figure 9 includes a sketch of the dominant gas dynamic features of the flow that are invisible in these direct plume images. When the chamber pressure is reduced, the wake zone becomes narrower and longer due to the greater expansion of the gas flow emanating from the nozzle. The internal shock wave grows, and its interaction point with the wake (at the maximum width of the wake) is pushed farther downstream. This effect is similar to what is observed when the nozzle pressure (P_0) is increased while P_a remains fixed (Mates and Settles, 2005b), which is the typical method employed in gas atomization to achieve finer atomization. As be-

TABLE 1: Isentropic flow conditions computed at experimental atomizing conditions

Expt.	P_0 [kPa] ($\pm$1%)[a]	P_{ac} [kPa] ($\pm$0.5%)	M	m_{gas} [kg/s] ($\pm$2%)	L_{sonic} [m]	u_{e} [m/s]	q [kPa]	Q [N]
B1	6290	104.8	3.33	0.167	0.571	656	815	110
B2	6290	104.1	3.34	0.167	0.574	656	812	110
VA1	6500	73.1	3.61	0.173	0.752	671	666	116
VA2	6470	73.0	3.61	0.172	0.751	671	665	115

[a] Stated uncertainties reflect 95% confidence intervals.

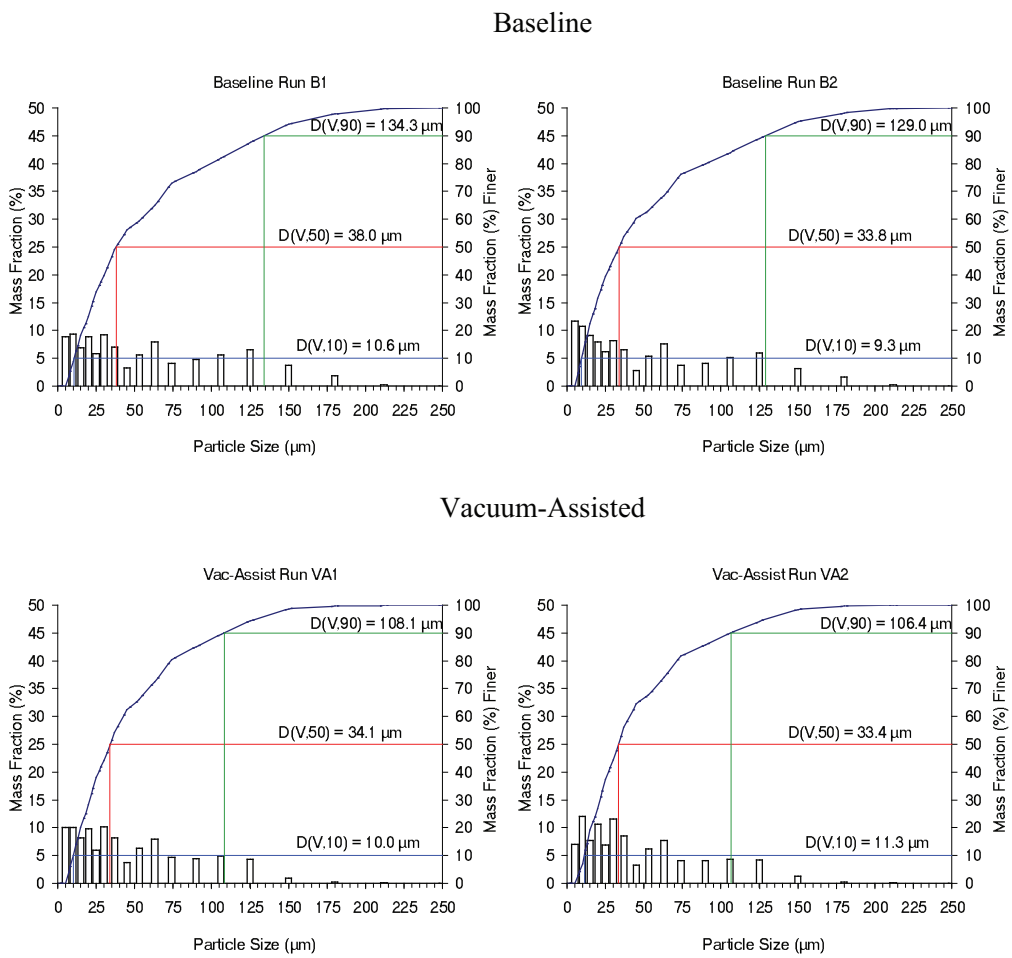

FIG. 9: Particle sieve analysis for baseline atomization runs (top) and vacuum-assisted runs (bottom).

fore, this underscores how the gas dynamic behavior of the atomization nozzle is fundamentally governed by the pressure ratio P_0/P_a, and not simply the nozzle pressure P_0.

Atomizing conditions and particle size data are shown in Table 2 for all experiments. Noted in the table is the pour temperature of each run, which is consistent for all runs. The particle size data presented consist of the weight fractions below the given particle diameter for material recovered below 250 µm. This material was subject to detailed particle size analysis by sieving. Also listed is the fraction of the total initial charge weight recovered that was larger than 250 µm. This oversize material consists mostly of solidified "splats" on the chamber walls, representing metal that was still molten at impact. Considering sub–250 µm material, the vacuum assist improved the yield of sub–45 µm

TABLE 2: Atomization parameters and mass-based particle size yields for baseline and vacuum-assisted runs

Expt.	P_0 [kPa] ($\pm$1%)[a]	P_a [kPa] ($\pm$0.5%)	T [°C] ($\pm$2%)	m_{metal} [kg/min] ($\pm$5%)	GMR	< 250 μm		% > 250 μm
						% < 125 μm	% < 45 μm	
B1	6290	104.8	1350	9.5	1.06	87.6	56.2	10.8
B2	6290	104.1	1350	7.4	1.35	89.1	60.3	5.1
VA1	6495	73.1	1350	10.0	1.04	94.4	62.5	11.0
VA2	6468	73.0	1350	9.1	1.14	94.2	64.6	18.3

[a] Stated uncertainties reflect 95% confidence intervals.

powder by 6.75% and the yield of sub–125 μm powder by 9.1%. Oversize yields are not included in the average particle diameter because they lie outside the sieve measurement range.

As Table 2 shows, while one vacuum-assisted run contained a reasonable percentage of >250 μm material (11.0%), the other run had a much higher proportion of material lost to "splats" (18.3%). Although it is impossible to estimate the size of the droplets that produced the splats, they are likely quite coarse since they remained molten all the way to the chamber wall. This suggests poorer atomization performance for this run. However, this conclusion must be tempered by the fact that convective heat transfer may be less effective under partial-vacuum conditions, which may tend to increase the propensity for the same size droplets to be molten at impact. The convective heat transfer coefficient, h, applicable for spheres in high Reynolds number flows, is given by Ranz and Marshall (1952):

$$h = \frac{k}{D}\left[2 + 0.6\text{Re}^{0.5}\text{Pr}^{0.33}\right]. \tag{8}$$

Here, k is the thermal conductivity of the gas, D is the sphere diameter, and Re and Pr are the Reynolds and Prandtl numbers, respectively. The effects of compressibility can be accounted for using an adiabatic wall temperature to evaluate the heat flux (White, 1986). Using Eq. (8), the heat transfer coefficient is decreased by 10% when P_a is reduced, primarily due to the reduction in Reynolds number. A more detailed analysis is beyond the scope of the present work. It is noteworthy that, if the material lost as splats is counted as >125 μm yield, the averaged vacuum-assist yield improvement of sub–125 μm powder falls to 2.6%, while the improvement in sub–45 μm powder falls to 0.5%.

Figure 9 plots the detailed sieve analysis of all four batches for the sub–250 μm powder. The most pronounced difference in the distributions produced under vacuum-assist is the reduced amount of the coarser particles in the distribution. The characteristic diameter which 90% of the particles by volume are smaller than, D(V, 90), averages 132 μm

for the normal runs while for the vacuum-assist runs it is 107 μm. That the D(V, 10) diameters are more comparable indicates that the vacuum-assist atomization reduces the frequency of coarser particles but achieves no improvement in the finest particle sizes, leading to a narrower overall particle size distribution. This result is consistent with the idea that a longer supersonic jet produces more complete secondary atomization. An aerodynamically limited atomization process is envisioned in which the gas velocity does not decay at all by the time secondary atomization is completed and all of the liquid is reduced to drop sizes below the stability limit determined from nozzle exit conditions. Under this condition one would obtain the finest mean diameter and narrowest particle size distribution possible for given nozzle exit conditions. This state of maximum might exist at some limiting GMR where further increases in GMR have no measureable effect on particle size. However, as will be argued here, GMR may not be the most appropriate parameter to capture the axial length scale effect in this type of atomization process.

Because reducing P_a has many effects on the driving force for atomization besides an elongated supersonic jet, as outlined in Table 1, it is simplistic to attribute the observed particle size refinement entirely to an increase in supersonic length alone. Two additional effects stand out besides the increased supersonic jet length. First, convective heat transfer from the droplets to the gas is reduced, as discussed earlier, which tends to increase the opportunity for breakup. Second, as mentioned previously, because the dynamic pressure of the gas flow, q, is reduced under vacuum-assist, the maximum stable droplet size increases according to the well-known Weber number (We) criterion (Lane, 1951). The Weber number is defined as

$$\mathrm{We} = \frac{qD}{\sigma}. \tag{9}$$

Here D is a characteristic liquid drop diameter and σ is the liquid surface tension. Aerodynamic instability begins at a critical value $\mathrm{We}_{\mathrm{crit}}$, which implies a maximum stable droplet size of D_{crit}. So as q increases, D_{crit} decreases, yielding finer atomization. These two effects thus tend to counterbalance one another. Numerical simulation is needed to sort out these effects. All that can be stated for certain is that the vacuum-assist led to measureable refinement in particle size in a manner that is consistent with more effective secondary breakup.

Finally, in Table 3, several highly cited empirical models are compared for co-axial, co-flowing twin-fluid atomizers. These models are used now only for rule-of-thumb estimates of atomization performance that can be readily evaluated, their role in atomizer design and detailed analysis having been replaced by the more powerful computational fluid dynamics techniques. Nevertheless, these models represent the collective behavior of significant amounts of experimental data obtained over more than 70 years. Here they are used to predict the relative influence of P_a on particle size for the present experiments. The equations are cast in terms of variable definitions already introduced, with

TABLE 3: Predicted effect of vacuum-assist on particle size trend from highly cited empirical equations developed over the past 70 years

Equation	Ref.	Year	Characteristic Diameter	Predicted Effect of Vacuum-Assist
$d = \frac{C_1}{u_\mathrm{e}}\sqrt{\frac{\sigma}{\rho_\mathrm{l}}} + C_2\left[\frac{\mu_\mathrm{l}}{\sqrt{\sigma\rho_\mathrm{l}}}\right]^{0.45}\left[\frac{C_3}{\mathrm{GMVR}}\right]^{1.5}$	21	1938	SMD	decrease
$d = d_0 C_1\left[\frac{\mu_\mathrm{l}}{\mu_\mathrm{g}}\left(\frac{\rho_E}{\rho_\mathrm{l}}\right)^2\frac{1}{\mathrm{We}}\left(1+\frac{1}{\mathrm{GMR}}\right)\right]^{0.5}$	18	1970	D(V, 50)	increase
$d = \frac{C_1}{q^{C_2}} + \frac{C_3}{\mathrm{GMR}^{C_4}}$	19	1971	D(V, 50)	increase
$d = d_0 C_1 / \left[1 + \frac{C_2\mathrm{We}}{1+\frac{1}{\mathrm{GMR}}}\right]$	20	1989	D(V, 50)	increase
$d = C_1\frac{\sigma}{\sqrt{\mathrm{GMVR}}}$	22	2001	D(V, 50)	decrease

the exception of the liquid surface tension, σ, and viscosity, μ, and density, ρ, of the liquid and gas (denoted by subscripts l and g, respectively). The variable d represents an average particle diameter, with d_0 a characteristic length scale, generally the diameter of the liquid orifice. Finally, the gas-to-metal volume ratio is denoted by GMVR. This term is analogous to GMR, but it is based on volume fluxes instead of mass fluxes. Since we are concerned with the relative effect of aerodynamic conditions on atomization performance rather than predictions of particle size, only the signs of the ratios of d are determined for each model at conditions corresponding to the present experiments, with a positive ratio indicating an increase d and a negative ratio indicating a decrease in d. SMD denotes the Sauter Mean Diameter while D(V, 50) is the mass median diameter.

As Table 3 shows, only two models predict a decrease in median or Sauter mean particle diameter while the other three predict an increase. Equations that utilize mass flow ratio, GMR, predict an increased particle size resulting from the vacuum-assist due to the reduction in q, which also lowers the Weber number. Equations that use GMVR, however, correctly predict the observed trend. Under vacuum conditions, the gas volume flux for a given mass flux is higher owing to the lower density of the expanded jet, leading to a higher value of GMVR and thus a smaller mean particle diameter. That the present experimental results are supported by some past observations is encourag-

ing, although the experimental conditions underpinning the two models that predict the observed trend are not based on similar experimental conditions. In Dunkley (2001), the data include low-density atomizing gases including helium, based on data reported in Ünal (1989), and heated gas (Strauss, 1999), both of which show a decrease in mean particle size. In both cases a higher value of GMVR is obtained because of reduced gas density, which illustrates why the models based on volume flux ratio correctly predict the trend. Of course, there are other effects involved when using helium or heated gas besides reducing the gas density. Most striking is the gas velocity, which dramatically increases for a given Mach number according to Eq. (5). Heat transfer will also be affected. These aerodynamic effects are presumably captured by an empirical constant (Dunkley, 2001).

The question thus arises, is the GMVR parameter fundamentally related to the axial length scales that are here hypothesized to cause the observed particle size refinement? To explore this, consider a sonic nozzle with a fixed throat area operated with values of P_0 and P_a corresponding to the present experiments. To compute the mass flows, we use the following equation:

$$m_{\text{gas}} = \sqrt{\gamma}\left(\frac{2}{\gamma+1}\right)^{(\gamma+1)/(2\gamma-2)} \frac{A^* P_0}{\sqrt{RT_0}}. \tag{10}$$

Here A^* is the area of the sonic throat. Table 4 shows that neither heating the gas nor using helium over nitrogen significantly changes L_{sonic}, according to Eq. (2). Comparing hypothetical hot nitrogen and room temperature helium jets with the experimental ones, both show large increases in gas volume flux, which would tend to drive down particle size according to these equations, but little or no change in L_{sonic}, demonstrating that there is no link between gas volume flux and L_{sonic}. Thus, the ability of these equations to predict the trends observed is apparently fortuitous, and none of the empirical models in Table 3 correctly capture the behavior observed in the present experiments. Finally,

TABLE 4: Isentropic calculations comparing hypothetical behavior of heated nitrogen and helium jets under normal and vacuum-assist conditions

Gas	P_0 [kPa]	P_a [kPa]	M	T_0 [K]	m_{gas} [kg/s]	L_{sonic} [m]	u_{e} [m/s]	Gas Volume Flux [m^3/s]
Nitrogen (γ = 1.4)	6290	104.8	3.33	300	0.167	0.574	656	0.044
	6500	73.1	3.61	300	0.173	0.752	671	0.058
	6290	104.8	3.33	600	0.118	0.574	928	0.063
	6500	73.1	3.61	600	0.122	0.752	949	0.083
Helium (γ = 1.67)	6290	104.8	3.33	300	0.067	0.532	1579	0.155
	6500	73.1	3.61	300	0.070	0.707	1606	0.195

Table 4 indicates that reducing P_a may improve atomization performance if either helium or heated nitrogen is used.

Finally, these experiments point out that controlling P_a can alter the aerodynamic conditions driving this variety of twin-fluid atomization in ways that are not normally investigated. This has the potential to significantly expand the aerodynamic parameter space for atomization processing beyond what is routinely explored. The potential payoff is a greater control over particle size and size distribution, either in metal powder production or in other similar twin-fluid atomization processes.

4. CONCLUSION

This work has demonstrated the vacuum-assisted atomization of liquid metal. Underlying the effect is the influence of the exhaust chamber pressure on the length of the supersonic region of the gas jet extending away from the nozzle, which will tend to achieve more effective secondary breakup and thus a finer particle size distribution. In particular, this effect reduces the frequency of the coarsest particles in the distribution, without changing the size of the finest particles. As a result, vacuum-assist leads to a narrowing of the particle size distribution. Empirical models developed over the past 70 years to predict mean particle size generally fail to predict the proper trend of vacuum-assist because they do not properly account for the axial length scale effect due to both gas velocity decay and the physics of liquid breakup, which require time and distance to complete. This work illustrates the importance of this axial length scale in twin-fluid atomization performance, and suggests how it might be used to control the behavior of an atomizer in ways that have been virtually unexplored. Finally, it is critical to note that the vacuum-assist effect, and in general the axial length scale effect discussed here, are likely important only in a limited range of atomization conditions. In this range, possibly between $0.1 < \mathrm{GMR} < 10$ as suggested by Kim and Marshall (1971), turbulent mixing and liquid drag effects exacerbate the decay in relative velocity between gas and liquid before atomization is driven to its aerodynamic limit.

ACKNOWLEDGMENTS

The authors gratefully acknowledge the help of Paul Boyer, Rodney Jiggetts and Robert Parke for their assistance in this work at NIST and for years of dedicated service to the NIST SiGMA atomizer facility, which is now permanently decommissioned.

REFERENCES

Adelberg, M., Mean drop size resulting from the injection of a liquid jet into a high speed gas stream, *AIAA J.*, vol. **6**, pp. 1143–1147, 1968.

Anderson, I. E., Byrd, D., and Meyer, J., Highly tuned gas atomization for controlled preparation of coarse powder, *Mat.-Wiss. Werkstofftech.*, vol. **41**, pp. 504–512, 2010.

Ayers, J. D. and Anderson, I. E., Method for generating fine sprays of molten metal for spray coating and powder making, US Patent No. 4,619,845, 1986.

Biancaniello, F. S., Conway, J. J., Espina, P. I., Mattingly, G. E., and Ridder, S. D., Particle size measurement of inert gas atomized powder, *Mat. Sci. Eng., A*, vol. **124**, pp. 9–14, 1990.

Dombrowski N. and Johns, W. R., The aerodynamic instability and disintegration of viscous liquid sheets, *Chem. Eng. Sci.*, vol. **18**, pp. 203–214, 1963.

Dunkley, J. J., An analysis of the gas atomization process, in *Proc. of the Nice European Congress and Exhibition on Powder Metallurgy*, vol. **4**, p. 99, 2001.

German, R. M., *Powder Metallurgy & Particulate Materials Processing*, Metal Powder Industries Federation, Princeton, NJ, 2005.

Hsiang, L.-P. and Faeth, G. M., Drop properties after secondary breakup, *Int. J. Multiphas. Flow*, vol. **19**, pp. 721–735, 1993.

Kim, K. Y. and Marshall, Jr., W. R., Drop-size distributions from pneumatic atomizers, *AIChE J.*, vol. **17**, pp. 575–584, 1971.

Klar, E. and Fesko, J. W., Atomization, *Metals Handbook*, 9th ed., Vol. 7, American Society for Metals, Metals Park, OH, 1984.

Lane, W. R., Shatter of drops in streams of air, *Ind. Eng. Chem.*, vol. **43**, pp. 1312–1317, 1951.

Lasheras, J. C. and Hopfinger, E. J. Liquid jet instability and atomization in a coaxial gas stream, *Ann. Rev. Fluid Mech.*, vol. **32**, pp. 275–308, 2000.

Lawley, A., *Atomization: The Production of Metal Powders*, Metal Powder Industries Federation, Princeton, NJ, 1992.

Lefebvre, A. H., *Atomization and Sprays*, Hemisphere Publishing Corporation, New York, 1989.

Lefebvre, A. H., Twin-fluid atomization: Factors influencing mean drop size, Keynote Lecture, in *Proc. of the Fifth International Conference on Liquid Atomization and Spray Systems*, ed. H. G. Semerjian, NIST, Gaithersburg, MD, p. 49, 1991.

Lubanska, H., Correlation of spray ring data for gas atomization of liquid metals, *JOM-J. Met.*, pp. 45–49, 1970.

Markus, S. and Fritsching, U., Discrete break-up modeling of melt sprays, *Int. J. Powder Metall.*, vol. **42**, no. 4, pp. 23–32, 2006.

Mates, S. P. and Settles, G. S., A Study of liquid metal atomization using close-coupled nozzles, Part 1: Gas dynamic behavior, *Atomization Spray*, vol. **15**, pp. 19–40, 2005a.

Mates, S. P. and Settles, G. S., A Study of liquid metal atomization using close-coupled nozzles, Part 2: Atomization behavior, *Atomization Spray*, vol. **15**, pp. 41–60, 2005b.

Miller, R. S., Miller, S. A., and Wojcik, L. A., Close-Coupled Atomization Utilizing Nonaxisymmetric Melt Flow, US Patent No. 5,601,781, 1997.

Mullis, A. M., McCarthy, I. N., and Cochrane, R. F., High speed imaging of the flow during close-coupled gas atomisation: Effect of melt delivery nozzle geometry, *J. Mater. Process. Tech*., vol. **211**, pp. 1471–1477, 2011.

Nagamatsu, H. T., Sheer, Jr., R. E., and Horvay, G., Supersonic jet noise theory and experiments, NASA SP-207, 1969.

Nukiyama, S. and Tanasawa, Y., *Trans. Soc. Mech. Eng*., vol. **4–6**, no. 1–6, 1938–40.

Ranz, W. E. and Marshall, Jr., W. R., Evaporation from drops—Part I, *Chem. Eng. Prog*., vol. **48**, pp. 141–146, 1952.

Ridder, S. D., Measurement and control of metal flow-rate in a gas-metal atomizer, in *Advances in Powder Metallurgy & Particulate Materials, Part 3—Particulate Production & Binders*, Metal Powder Industries Federation, Princeton, N.J., 2002.

Ridder, S. D. and Biancaniello, F. S., Process control during high pressure atomization, *Mater. Sci. Eng.*, vol. **98**, pp. 47–51, 1988.

Ridder, S. D., Osella, S. A., Espina, P. I., and Biancaniello, F. S., Intelligent control of particle size distribution during gas atomization, *Int. J. Powder Metall*., vol. **28**, pp. 133–147, 1992.

Settles, G. S., *Schlieren and Shadowgraph Techniques*, Springer, Berlin, 2001.

Strauss, J. T., Hotter gas increases atomization efficiency, *Met. Powder Rpt.*, vol. **11**, pp. 24–28, 1999.

Thompson, J. S., A study of process variables in the production of aluminium powder by atomization, *J. Inst. Met.*, vol. **74**, pp. 101–132, 1948.

Tong, M. and Browne, D. J., Modelling compressible gas flow near the nozzle of a gas atomiser using a new unified model, I, *Comput. Fluids*, vol. **38**, pp. 1183–1190, 2009.

Ünal, A., Influence of nozzle geometry in gas atomisation of rapidly solidified aluminium alloys, *Mater. Sci. Tech.*, vol. **4**, pp. 909–915, 1988.

Ünal, A., Liquid break-up in gas atomization of fine aluminum powders, *Met. Trans., B*, vol. **20B**, pp. 61–69, 1989.

Ünal, A. and Robertson, D. G. C., Pilot plant gas atomizer for rapidly solidified metal powders, *Int. J. Rapid Solidif.*, vol. **2**, pp. 219–229, 1986.

Walz, A., Metal powders and a process for the production thereof, US Patent #4,534,917, 1984.

Wigg, L. D., Drop-size prediction for twin-fluid atomisers, *J. Inst. Fuel*, vol. **37**, pp. 500–505, 1964.

White, F. M., *Fluid Mechanics*, 2nd ed., McGraw-Hill, New York, 1986.

Yule, A. J. and Dunkley, J. J., *Atomization of Melts for Powder Production and Spray Deposition*, Oxford University Press, 1994.

Zeoli, N., Tabbara, H., and Gu, S., Three-dimensional simulation of primary break-up in a close-coupled atomizer, *Appl. Phys., A*, vol. **108**, pp. 783–792, 2012.

Zhao, W. J., Cao, F. Y., Ning, Z. L., Zhang, G. G., Li, Z., and Sun, J. F., A computational fluid dy-

namics (CFD) investigation of the flow field and the primary atomization of the close coupled atomizer, *Comput. Chem. Eng.*, vol. **40**, pp. 58–66, 2012.